



**HAL**  
open science

## Ferromagnetic Quasi-Two-Dimensional Electron Gas with Trigonal Crystal Field Splitting

Yu Chen, Maria D'antuono, Nicholas B. Brookes, Gabriella M. de Luca,  
Roberto Di Capua, Emiliano Di Gennaro, Giacomo Ghiringhelli, Cinthia  
Piamonteze, Daniele Preziosi, Benoit Jouault, et al.

► **To cite this version:**

Yu Chen, Maria D'antuono, Nicholas B. Brookes, Gabriella M. de Luca, Roberto Di Capua, et al.. Ferromagnetic Quasi-Two-Dimensional Electron Gas with Trigonal Crystal Field Splitting. *ACS Applied Electronic Materials*, 2022, 4 (7), pp.3226-3231. 10.1021/acsaelm.2c00447 . hal-04075124

**HAL Id: hal-04075124**

**<https://hal.science/hal-04075124>**

Submitted on 28 Nov 2023

**HAL** is a multi-disciplinary open access archive for the deposit and dissemination of scientific research documents, whether they are published or not. The documents may come from teaching and research institutions in France or abroad, or from public or private research centers.

L'archive ouverte pluridisciplinaire **HAL**, est destinée au dépôt et à la diffusion de documents scientifiques de niveau recherche, publiés ou non, émanant des établissements d'enseignement et de recherche français ou étrangers, des laboratoires publics ou privés.

# A ferromagnetic quasi-two-dimensional electron gas with trigonal crystal field splitting

*Yu Chen<sup>1\*\*</sup>, Maria D'Antuono<sup>1,2</sup>, Nicholas B. Brookes<sup>3</sup>, Gabriella M. De Luca<sup>1,2</sup>, Roberto Di Capua<sup>1,2</sup>, Emiliano Di Gennaro<sup>1,2</sup>, Giacomo Ghiringhelli<sup>4,5</sup>, Cinthia Piamonteze<sup>6</sup>, Daniele Preziosi<sup>7</sup>, Benoit Jouault<sup>8</sup>, Mariona Cabero<sup>9</sup>, José María González-Calbet<sup>9</sup>, Carlos León<sup>10</sup>, Jacobo Santamaria<sup>10</sup>, Alessia Sambri<sup>1</sup>, Daniela Stornaiuolo<sup>1,2</sup> and Marco Salluzzo<sup>1\*</sup>*

<sup>1</sup>CNR-SPIN, Complesso Monte Sant'Angelo via Cinthia, I-80126 Napoli, Italy

<sup>2</sup>Dipartimento di Fisica "E. Pancini", Università di Napoli "Federico II", Complesso Monte Sant'Angelo via Cinthia, I-80126 Napoli, Italy

<sup>3</sup>ESRF—The European Synchrotron, 71 Avenue des Martyrs, CS 40220, F-38043 Grenoble, France

<sup>4</sup>Dipartimento di Fisica Politecnico di Milano, Piazza Leonardo da Vinci 32, I-20133 Milano, Italy

<sup>5</sup>CNR-SPIN, Politecnico di Milano, Piazza Leonardo da Vinci 32, I-20133 Milano, Italy

<sup>6</sup>Photon Science Division, Paul Scherrer Institut, CH-5232 Villigen PSI, Switzerland.

<sup>7</sup>Université de Strasbourg, CNRS, IPCMS UMR 7504, 67034 Strasbourg, France

<sup>8</sup>Laboratoire Charles Coulomb, UMR 5221, CNRS, Université de Montpellier, F-34095

Montpellier, France

<sup>9</sup>Centro Nacional de Microscopia Electronica. Universidad Complutense 28040 Madrid, Spain

<sup>10</sup>GFMC. Dept. Fisica de Materiales. Facultad de Fisica. Universidad Complutense. 28040

Madrid, Spain

**ABSTRACT:** Interfacial inversion symmetry breaking gives rise to electronic properties that differ substantially from those of the bulk constituent materials. Here we report on the realization of an artificial ferromagnetic quasi-two-dimensional electron gas (q2DEG) at the (111) interfaces between LaAlO<sub>3</sub>, EuTiO<sub>3</sub> and SrTiO<sub>3</sub> characterized by a reconstruction of the bulk quasi-octahedral crystal field into a trigonal one. The q2DEG is created through a transfer of electrons to the EuTiO<sub>3</sub> layers at the interface with LaAlO<sub>3</sub>, extending into the first layers of SrTiO<sub>3</sub>, as shown by electron energy loss spectroscopy map of the titanium valence with atomic column resolution. Interestingly, polarized x-ray absorption spectroscopy shows that the Eu-4*f* and the Ti-3*d* magnetic moments order ferromagnetically and exhibit the same magnetic field dependence at low temperature. In addition, the q2DEG presents a sizable in-plane orbital moment even at low magnetic field (0.1 Tesla) possibly related to Ti-3*d* electrons occupying bands with main *a<sub>1g</sub>* orbital character. The results show an intriguing interplay between ferromagnetism, spin-orbit coupling and trigonal crystal field splitting in the (111) LaAlO<sub>3</sub>/EuTiO<sub>3</sub>/SrTiO<sub>3</sub> q2DEG.

**KEYWORDS:** ferromagnetic q2DEG, trigonal crystal field, XMCD, EELS, Ti-3*d* orbitals, (111) STO, LAO/ETO/STO

## **Introduction**

The discovery of a quasi-two-dimensional electron gas (q2DEG) at the (001) interface between  $\text{LaAlO}_3$  (LAO) and  $\text{SrTiO}_3$  (STO) band insulators<sup>1,2</sup> generated a widespread interest due to the remarkable and sometimes unexpected properties,<sup>3</sup> alike gate tunable (unconventional) superconductivity,<sup>4-7</sup> arising from the interplay between a rather strong Rashba-like spin-orbit coupling<sup>8,9</sup> and an intrinsic multi-band transport associated to non-degenerate Ti-3d  $t_{2g}$  bands. Moreover, two-dimensional magnetism, coexisting with superconductivity, can be induced by opportune atomic engineering of the heterostructures.<sup>10</sup> All these phenomena are related to interfacial orbital reconstructions which dominate the oxide q2DEGs physics.<sup>11,12</sup>

Recently, (111) LAO/STO interfaces attracted substantial interest due to the reconstruction of the bulk quasi-octahedral crystal field into a trigonal one<sup>13</sup> and to the possible role of electronic correlations, which need to be further studied to explain their intriguing electronic properties.<sup>14, 15</sup> At the (111) interface, the octahedral ( $O_h$ ) and quasi-octahedral ( $D_{4h}$ ) symmetry of bulk STO and of (001) or (110) STO 2DEGs, respectively, turn into a  $D_{3d}$  symmetry, where the crystal field is trigonal (Fig. 1a) owing to the hexagonal surface lattice.<sup>13</sup> Within the  $D_{3d}$  symmetry, the  $t_{2g}$  orbitals ( $3d_{xy}$ ,  $3d_{yz}$ ,  $3d_{zx}$ ) mix and transform into  $a_{1g}$  and  $e_g^\pi$  states (Fig. 1b). The latter can be further split through distortion along the (111) axis and by the spin-orbit coupling.<sup>16</sup> Consequently, the band structure of (111) oxide heterostructures is susceptible to being more significantly altered at the interfaces with respect to the (001) and (110) cases. Indeed, (111) LAO/STO q2DEGs exhibit some intriguing properties, like a reduced superconducting critical temperature and intrinsic anomalous Hall effect related to the topology of the band structure and their Berry curvature.<sup>17, 18</sup>

In this manuscript we report on the electronic properties and the magnetism in the artificial spin-polarized q2DEG realized by introducing few unit cells (uc) of  $\text{EuTiO}_3$ , an antiferromagnetic

insulator isostructural to STO, between a LAO epitaxial film and a Ti-terminated (111) STO single crystal.

By using x-ray magnetic circular dichroism (XMCD) at the Ti-3*d* L<sub>2,3</sub> and Eu-4*f* M<sub>4,5</sub> edges, complemented by quantum interference device (SQUID) magnetometry, we provide evidence of a ferromagnetic (FM) order originating from the correlation between Ti- and Eu- magnetic moments in this system. Furthermore, we show a sizeable Ti-orbital moment oriented primarily along the in-plane direction that, together with an anisotropic magnetization, suggests an intriguing spin-orbit texture stemming from the interplay between the trigonal crystal field splitting of the low lying *a<sub>1g</sub>* and *e<sub>g</sub><sup>π</sup>* bands, the spin-orbit coupling and the magnetism in this oxide q2DEG.

## Experimental Results

LAO/ETO/STO heterostructures were prepared by pulsed laser deposition (PLD) assisted by specular reflection high energy electron diffraction (RHEED). In a background oxygen pressure of  $0.8 \times 10^{-5}$  mbar at 720 °C and laser fluence of 1.3 J/cm<sup>2</sup>, 3 uc-thick ETO film and 10 uc-thick LAO film were sequentially grown epitaxially on Ti-terminated (111) STO single crystals pre-processed by buffered hydrofluoric acid etching and oxygen annealing.<sup>19</sup> The average number of layers along the [111] direction was monitored by the oscillations of the specular RHEED intensity (see Figure 2a). Each oscillation corresponds to a thickness equal to the distance ( $d=a/\sqrt{3}$ , *a* is the lattice constant) between two Ti/Eu (for ETO, *d* ~ 0.23 nm) and Al/La (for LAO, *d* ~ 0.22 nm) layers along [111] direction. Real time RHEED oscillations (Fig. 2a) show that the film growth proceeds layer-by-layer, while Atomic Force Microscopy (AFM, Fig. 2b) confirms that the LAO/ETO/STO surface is composed of step-terraces with a height of ~0.22 nm, similar to the pristine STO (see Supporting Information, SI, Note 1 and SI Figure S1).

High resolution aberration corrected electron microscopy and spectroscopy revealed the high structural quality of the LAO/ETO/STO heterostructures. Fig. 2c displays an annular dark field (ADF) image of a (111) LAO/ETO/STO sample. The layers look homogeneous with no sign of mismatch dislocations, evidencing the epitaxial growth of the heterostructure. The images reveal a sharp interface between ETO and STO, while the LAO/ETO interface is less defined due to similar (atomic number) Z-contrast of La and Eu.

On the other hand, both interfaces are clearly discerned in the right panel of Fig. 2c, which shows false colour La, Eu and Ti elemental maps obtained by electron energy loss spectroscopy (EELS) at Ti L<sub>2,3</sub>, La M<sub>4,5</sub> and Eu M<sub>4,5</sub> absorption edges. Composition profiles and EELS show some La/Eu intermixing at the LAO/ETO interface, and a negligible Ti interdiffusion into the LAO film, as shown in SI Figures S2 and S3. The effective average thickness of the ETO layer estimated from the Eu-EELS line scans is about 3-4 Eu rows, thus comparable to the average number of layers as expected from the deposition rate and RHEED analysis (See Fig. 2a). At the LAO/ETO interface, we do see an intermixed unit cell where Eu and La are partially exchanged. Some Eu migrate also in the LAO layer, which can be clearly distinguished from ETO in the line scans by the abrupt reduction of the titanium signal in the EELS maps (SI Figures S2 and S3). The Eu-fraction replacing La, from the EELS line scan, is roughly 20% in the first nm at the interface.

Changes of the local Ti oxidation state across the LAO/ETO/STO interfaces have been investigated by O-K near-edge EELS fine structure (see SI Figure S3). Fig. 2d shows a laterally averaged Ti-valence profile as a function of the spatial coordinate along the interface direction (the error bars in the figure correspond to the standard deviation of the measurement). While in the STO substrate the Ti valence is near to the nominal +4 value, starting from the first two STO unit cells at the interface with ETO it is gradually reduced to a minimum of +3.8 in the first ETO layer

at the interface with LAO. This reduction of the Ti oxidation state is related to the partial La/Eu intermixing, which can provide electron doping in the ultrathin ETO layer<sup>20</sup>, and to the presence of a conducting q2DEG.

The LAO/ETO/STO q2DEG exhibits a metallic temperature dependence of the sheet resistance down to 4.2 K with low temperature values in the 0.6-0.8 K $\Omega$  range, comparable to standard (001) LAO/STO<sup>6</sup> and (001) LAO/ETO/STO heterostructures.<sup>10,21</sup> The sheet resistance of the q2DEG can be strongly modulated by back-gating using electric field effect (Fig. 3a). At zero gate voltage the resistance shows a small upturn, possibly related to weak-localization effects, like in (001) LAO/STO and LAO/ETO/STO heterostructures<sup>8-10</sup> and (111) LAO/STO interfaces.<sup>14</sup> When a positive gate voltage is applied, on the other hand, the resistance shows a metallic temperature dependence with a drop below 8-10 K, possibly related to a FM ordering (see Fig. 3b), similar to (001) LAO/ETO/STO q2DEGs.<sup>10,21</sup>

In order to study the crystal field splitting and the magnetism in our heterostructures, we used polarization dependent x-ray absorption spectroscopy (XAS) across the Eu-M<sub>4,5</sub> and the Ti-L<sub>2,3</sub> edges. The experiments were performed at the beamline X-Treme of the Swiss Light Source<sup>22</sup> and at the beamline ID32 of the European Synchrotron Research Facility (ESRF).<sup>23, 24</sup> XAS performed with circularly or linearly polarized photons can detect the magnetic moments and the 3d orbital crystal field splitting, respectively. The two techniques, usually known as XMCD and x-ray linear dichroism (XLD) are so sensitive that they can be used on a single interface. The samples were mounted with the (111) surface in the vertical laboratory plane, and the vertical axis parallel to the [10 $\bar{1}$ ] crystallographic direction determined by x-ray diffraction, i.e., parallel to one of the three equivalent Ti-Ti bonds within the hexagonal surface lattice (Fig. 3c). The energy resolution at both

beamlines was around 100 meV. XAS, XLD and XMCD spectra were compared to theoretical spectra obtained by atomic multiplet scattering calculations using the CTM4XAS code.<sup>25</sup>

The orbital crystal field symmetry and splitting, of the (111) LAO/ETO/STO q2DEG, were obtained from the analysis of XLD spectra, determined as the difference of XAS spectra acquired with linear polarizations along the horizontal (H) and vertical (V) directions in the laboratory frame,  $XLD = I_H - I_V$ . In Fig. 3d we present a typical XLD spectrum measured in grazing incidence conditions (GI,  $\theta=60$  degrees from the surface normal). The XLD of (111) heterostructures differ notably from the typical one measured on (001) interfaces (see SI Figure S4).<sup>11,13</sup> It can be reproduced by atomic multiplet scattering calculations only by using a trigonal crystal field symmetry ( $D_{3d}$ ), and a splitting of 20 meV between the (lowest)  $a_{1g}$  and  $e_g^\pi$  orbitals. Since the total electron yield (TEY) probing depth is between 2-3 nm at the Ti-edge, the results suggest that not only the interface layer, but also the ETO and the first STO unit cells exhibit a trigonal crystal field, in spite of the quasi- $O_h$  symmetry in bulk STO. The trigonal crystal field reflects in the presence of at least two non-degenerate bands originating from the trigonal  $a_{1g}$  and  $e_g^\pi$  orbitals, corresponding to  $J=1/2$  and  $J=3/2$  doublet and quartet respectively.

To further elucidate the effect of the trigonal symmetry on the magnetic properties of this heterostructure, we studied the magnetism of the (111) LAO/ETO/STO q2DEG by using XMCD at the Eu-M<sub>4,5</sub> and the Ti-L<sub>2,3</sub> edges. In Fig. 4a we show typical large field (6.5 Tesla) XMCD spectra acquired in GI conditions. Alike (001) LAO/ETO/STO q2DEG,<sup>10,21</sup> (111) LAO/ETO/STO shows a strong XMCD at both Eu-M<sub>4,5</sub> and the Ti-L<sub>2,3</sub> edges. The Eu-spin moment, obtained from the sum rules, is of the order of 4  $\mu_B$ /Eu, lower than the 7  $\mu_B$ /Eu value expected for Eu<sup>2+</sup> states, suggesting the presence of a fraction of Eu in the non-magnetic Eu<sup>3+</sup> configuration. This result

agrees with the EELS data, which show some Eu/La substitution inside the LAO layer, where Eu get an  $\text{Eu}^{3+}$  valence, explaining the reduced value of the XMCD.

The overall shape of the XMCD spectra can be reproduced by atomic multiplet simulations for  $\text{Eu}^{2+}$  and  $\text{Ti}^{4+}$  ions in  $C_3$  symmetry. However, while a positive exchange is needed to simulate the  $\text{Eu}^{2+}$  magnetization, parallel to the magnetic field, only a negative one correctly reproduces the Ti-XMCD peaks at  $L_3$  and  $L_2$ , analogous to the (001) interface (see refs. [10, 20]).

Furthermore, we also find a finite and positive Ti-XMCD integral which, according to the sum rules,<sup>26</sup> indicates a sizeable Ti- $3d$  orbital moment,  $m_{orb}$ , up to  $-0.025 \mu_B/\text{Ti}$ . The finite XMCD integral, unexpected for empty Ti- $3d^0$  orbitals, is related to a small fraction of  $\text{Ti}^{3+}$  (Ti- $3d^1$ ) electronic states which contribute to the finite magnetic (orbital and spin) moment. The result qualitatively agrees with the Ti valence profile measured by EELS across the LAO/ETO/STO interface, suggesting the presence of Ti- $3d^1$  electrons within the ETO and in the first unit cells of the STO.

In Fig. 4b we report Ti-XMCD spectra and XMCD-integral at 0.1 Tesla as function of the angle  $\theta$ . The data show a sizeable XMCD also at this low magnetic field, and an orbital moment, which progressively increases with the angle  $\theta$  and changes sign at normal incidence ( $\theta=0$ ). In Figs. 4c,d we show the magnetic field dependence of the Eu- $M_5$  and Ti- $L_3$  XMCD intensity, proportional to the magnetization, measured at 2 K in normal and GI conditions. The data show that the XMCD is anisotropic, with a preferred in-plane orientation, and saturates above 2-3 Tesla. Moreover, the XMCD intensities acquired at the two edges are clearly correlated, since they have a similar magnetic field dependence, suggesting a magnetic coupling between Eu- $4f$  and Ti- $3d$  states.

In order to establish if the system is ferromagnetic, we show in Fig. 4e a magnetic hysteresis loop at 2 K obtained by SQUID magnetometry. The data shows the presence of a hysteresis at low

field when the field is parallel to the interface, which suggests FM correlations in the plane of the q2DEG. On the other hand, no hysteresis was observed for a magnetic field perpendicular to the interface.

In Fig. 4f we show the angular dependence of the Eu ( $m_{spin}$ ) and Ti ( $m_{orb}$ ) orbital magnetic moments at 0.1 Tesla and 2 K obtained using the sum rules. The data confirm that the Ti-3*d* orbital moment decreases as a function of the angle  $\theta$ , and changes sign in normal incidence, indicating that the Ti and Eu spin moment (according to the Hund's rules) are parallel (and directed along the magnetic field) in GI conditions, but antiparallel in normal incidence. One of the possible Eu-spin configurations, which can explain the absence of a finite out-of-plane magnetization, is shown in the inset of Fig. 4f. The idea is that Eu-spin moments are canted out-of-plane by the perpendicular magnetic field in alternating up and down sequences, so that no net out-of-plane magnetization is observed at zero field.

These results suggest that the magnetism in (111) LAO/ETO/STO is rather complex and characterized by possibly non-collinear spins, with a FM ordering of the in-plane magnetic moment component, in agreement with the presence of a clear hysteresis only for a field parallel to the interface, and a FM coupling between Ti-3*d* and Eu-4*f* moments in the plane. On the other hand, the coupling between Ti and Eu magnetic moments switches to antiferromagnetic in the out-of-plane direction, where also no hysteresis is observed in the XMCD and SQUID magnetization loops, suggesting a complex spin-texture which deserves further theoretical and experimental studies.

## **Conclusions**

We have demonstrated the formation of a ferromagnetic q2DEG at the (111) LAO/ETO/STO interface characterized by a reconstruction of the bulk quasi-octahedral crystal field into a trigonal field. Atomic resolved electron energy loss spectroscopy shows that the q2DEG is located in the EuTiO<sub>3</sub> layers and extends into the first layers of SrTiO<sub>3</sub>. Furthermore, we found an intriguing angular dependence of the Ti-orbital moment, suggesting a sizable in-plane moment and in-plane ferromagnetic correlations. The study on the (111) LaAlO<sub>3</sub>/EuTiO<sub>3</sub>/SrTiO<sub>3</sub> q2DEG reveals an intriguing interplay between ferromagnetism, spin-orbit coupling and trigonal crystal field.

## **Methods**

### **Samples preparation**

LAO(10 uc)/ETO(3 uc)/STO(111) heterostructures were fabricated by PLD assisted by RHEED from sintered Eu<sub>2</sub>Ti<sub>2</sub>O<sub>7</sub> and crystalline LAO targets onto TiO<sub>2</sub>-terminated (111) STO substrates pre-processed by buffered hydrofluoric acid etching and oxygen annealing. The samples were deposited using an excimer laser (Lambda Physics, 248 nm wavelength) and 1.3 J/cm<sup>2</sup> fluence, 1 Hz of repetition, in a background O<sub>2</sub> pressure of 8×10<sup>-5</sup> mbar at a temperature of 720 °C and cooled down in the same conditions to room temperature with a rate of 5 °C/min.

### **Electron microscopy**

Specimens were prepared by grinding and Ar ion milling. Sample structure was characterized by STEM at Centro Nacional de Microscopia Electronica, Universidad Complutense, Madrid. Z-contrast images were obtained in a NionUltraSTEM operated at 100 kV and equipped with a 5th order corrector and a Gatan Enfina spectrometer capable of simultaneous AFD imaging and EELS at Ti L<sub>2,3</sub>, La M<sub>4,5</sub> and Eu M<sub>4,5</sub> absorption edges.

### **XAS, XLD and XMCD spectroscopy measurements**

The experiments of polarization dependent x-ray absorption spectroscopy (XAS) across the Eu-M<sub>4,5</sub> and the Ti-L<sub>2,3</sub> edges were performed at the beamline X-Treme of the Swiss Light Source<sup>22</sup> and at the beamline ID32 of the European Synchrotron Research Facility (ESRF).<sup>23, 24</sup> XAS performed with circularly or linearly polarized photons can detect the magnetic moments and the 3d orbital crystal field splitting, respectively. The samples were mounted with the (111) surface in the vertical laboratory plane, and the vertical axis parallel to the [10 $\bar{1}$ ] crystallographic direction determined by x-ray diffraction, i.e., parallel to one of the three equivalent Ti-Ti bonds within the hexagonal surface lattice (Fig. 3c). The energy resolution at both beamlines was around 100 meV. XAS, XLD and XMCD spectra were compared to theoretical spectra obtained by atomic multiplet scattering calculations using the CTM4XAS code.<sup>25</sup>

### **SQUID magnetometry measurement**

SQUID data were collected by using a Quantum Design MPMS3 magnetometer at the Université de Strasbourg, IPCMS. Magnetization measurements as a function of magnetic field were acquired on LAO/ETO//STO heterostructure. Data were corrected for the diamagnetism of the substrate substrating the linear contribution acquired at high magnetic fields.

### **Corresponding Authors**

\* [marco.salluzzo@spin.cnr.it](mailto:marco.salluzzo@spin.cnr.it)

\*\*[yu.chen@spin.cnr.it](mailto:yu.chen@spin.cnr.it)

## Author Contributions

Conceptualization: MS. Sample preparation: YC, AS, EDG, MS, RDC. Transport measurements and Analysis: BJ, DS, YC, MDA. STEM and EELS Experiment: MC, J G-C, CL, JS. XMCD Experiment: and Analysis: CP, MS, GG, GMDL, DP. SQUID Experiment: DP. Supervision: MS. Writing: MS, YC. Writing-review & editing: all the Authors participated to the editing of the paper.

## ACKNOWLEDGMENTS

This project received funding from the ERA-NET QUANTERA European Union's Horizon H2020 project QUANTOX under Grant Agreement No. 731473, from the Ministero dell'Istruzione, dell'Università e della Ricerca for the PRIN project TOP-SPIN (Grant No. PRIN 20177SL7HC). DP has benefited support from the initiative of excellence IDEX-Unistra (ANR-10-IDEX-0002-02) from the French national program Investment for the future. We acknowledge discussion with R. Citro, M. Cuoco, A. Filippetti and A. Perroni.

## REFERENCES

- (1) Ohtomo, A.; Hwang, H. Y. A High-Mobility Electron Gas at the LAO/STO Heterointerface. *Nature* **2004**, *427*, 423.
- (2) Thiel, S.; Hammerl, G.; Schmehl, A.; Schneider, C. W.; Mannhart, J. Tunable Quasi-Two-Dimensional Electron Gases in Oxide Heterostructures. *Science* **2006**, *313*, 1942–1945.
- (3) Brinkman, A.; Huijben, M.; Van Zalk, M.; Huijben, J.; Zeitler, U.; Maan, J. C.; Van Der Wiel, W. G.; Rijnders, G.; Blank, D. H. A. a; Hilgenkamp, H. Magnetic Effects at the Interface between Non-Magnetic Oxides. *Nat. Mater.* **2007**, *6*, 493–496.

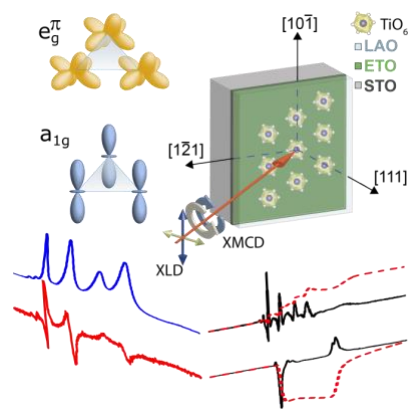
- (4) Caviglia, A. D.; Gariglio, S.; Reyren, N.; Jaccard, D.; Schneider, T.; Gabay, M.; Thiel, S.; Hammerl, G.; Mannhart, J.; Triscone, J. M. Electric Field Control of the LaAlO<sub>3</sub>/SrTiO<sub>3</sub> Interface Ground State. *Nature* **2008**, *456*, 624.
- (5) Richter, C.; Boschker, H.; Dietsche, W.; Fillis-Tsirakis, E.; Jany, R.; Loder, F.; Kourkoutis, L. F.; Muller, D. A.; Kirtley, J. R.; Schneider, C. W.; Mannhart, J. Interface Superconductor with Gap Behaviour like a High-Temperature Superconductor. *Nature* **2013**, *502*, 528.
- (6) Stornaiuolo, D.; Massarotti, D.; Di Capua, R.; Lucignano, P.; Pepe, G. P.; Salluzzo, M.; Tafuri, F. Signatures of Unconventional Superconductivity in the LaAlO<sub>3</sub> / SrTiO<sub>3</sub> Two-Dimensional System. *Phys. Rev. B* **2017**, *95*, 140502.
- (7) Ben Shalom, M.; Sachs, M.; Rakhmilevitch, D.; Palevski, A.; Dagan, Y. Tuning Spin-Orbit Coupling and Superconductivity at the SrTiO<sub>3</sub>/LaAlO<sub>3</sub> Interface: A Magnetotransport Study. *Phys. Rev. Lett.* **2010**, *104*, 126802.
- (8) Caviglia, A. D.; Gabay, M.; Gariglio, S.; Reyren, N.; Cancellieri, C.; Triscone, J. M. Tunable Rashba Spin-Orbit Interaction at Oxide Interfaces. *Phys. Rev. Lett.* **2010**, *104*, 126803.
- (9) Stornaiuolo, D.; Gariglio, S.; Fête, A.; Gabay, M.; Li, D.; Massarotti, D.; Triscone, J. M. Weak Localization and Spin-Orbit Interaction in Side-Gate Field Effect Devices at the LaAlO<sub>3</sub>/SrTiO<sub>3</sub> Interface. *Phys. Rev. B* **2014**, *90*, 235426.
- (10) Stornaiuolo, D.; Cantoni, C.; De Luca, G. M.; Di Capua, R.; Di Gennaro, E.; Ghiringhelli, G.; Jouault, B.; Marrè, D.; Massarotti, D.; Granozio, F. M.; Pallecchi, I.; Piamonteze, C.; Rusponi, S.; Tafuri, F.; Salluzzo, M. Tunable Spin Polarization and Superconductivity in

Engineered Oxide Interfaces. *Nat. Mater.* **2016**, *15*, 278.

- (11) Salluzzo, M.; Cezar, J. C.; Brookes, N. B.; Bisogni, V.; De Luca, G. M.; Richter, C.; Thiel, S.; Mannhart, J.; Huijben, M.; Brinkman, A.; Rijnders, G.; Ghiringhelli, G. Orbital Reconstruction and the Two-Dimensional Electron Gas at the LaAlO<sub>3</sub>/SrTiO<sub>3</sub> Interface. *Phys. Rev. Lett.* **2009**, *102*, 166804.
- (12) Salluzzo, M.; Gariglio, S.; Stornaiuolo, D.; Sessi, V.; Rusponi, S.; Piamonteze, C.; De Luca, G. M.; Minola, M.; Marré, D.; Gadaleta, A.; Brune, H.; Nolting, F.; Brookes, N. B.; Ghiringhelli, G. Origin of Interface Magnetism in BiMnO<sub>3</sub>/SrTiO<sub>3</sub> and LaAlO<sub>3</sub>/SrTiO<sub>3</sub> Heterostructures. *Phys. Rev. Lett.* **2013**, *111*, 087204.
- (13) De Luca, G. M.; Di Capua, R.; Di Gennaro, E.; Sambri, A.; Granozio, F. M.; Ghiringhelli, G.; Betto, D.; Piamonteze, C.; Brookes, N. B.; Salluzzo, M. Symmetry Breaking at the (111) Interfaces of SrTiO<sub>3</sub> Hosting a Two-Dimensional Electron System. *Phys. Rev. B* **2018**, *98*, 115143.
- (14) Monteiro, A. M. R. V. L.; Vivek, M.; Groenendijk, D. J.; Bruneel, P.; Leermakers, I.; Zeitler, U.; Gabay, M.; Caviglia, A. D. Band Inversion Driven by Electronic Correlations at the (111) LaAlO<sub>3</sub>/SrTiO<sub>3</sub> Interface. *Phys. Rev. B* **2019**, *99*, 201102.
- (15) Rout, P. K.; Maniv, E.; Dagan, Y. Link between the Superconducting Dome and Spin-Orbit Interaction in the (111) LaAlO<sub>3</sub>/SrTiO<sub>3</sub> Interface. *Phys. Rev. Lett.* **2017**, *119*, 237002.
- (16) Trama, M.; Cataudella, V.; Perroni, C. A. Strain-Induced Topological Phase Transition at (111) SrTiO<sub>3</sub>-Based Heterostructures. *Phys. Rev. Res.* **2021**, *3*, 043038.

- (17) Lesne, E.; Sağlam, Y. G.; Battilomo, R.; van Thiel, T. C.; Filippozzi, U.; Cuoco, M.; Steele, G. A.; Ortix, C.; Caviglia, A. D. Designing Berry Curvature Dipoles and the Quantum Nonlinear Hall Effect at Oxide Interfaces. *arXiv* **2022**, <https://doi.org/10.48550/arXiv.2201.12161>.
- (18) Trama, M.; Perroni, C. A.; Cataudella, V.; Romeo, F.; Citro, R. Gate Tunable Anomalous Hall Effect at (111) LaAlO<sub>3</sub>/SrTiO<sub>3</sub> Interface. *arXiv* **2022**, <http://arxiv.org/abs/2202.04664>.
- (19) Torrelles, X.; Cantele, G.; De Luca, G. M.; Di Capua, R.; Drnec, J.; Felici, R.; Ninno, D.; Herranz, G.; Salluzzo, M. Electronic and Structural Reconstructions of the Polar (111) SrTiO<sub>3</sub> Surface. *Phys. Rev. B* **2019**, *99*, 205421.
- (20) Katsufuji, T.; Tokura, Y. Transport and Magnetic Properties of a Ferromagnetic Metal: Eu<sub>1-x</sub>R<sub>x</sub>TiO<sub>3</sub>. *Phys. Rev. B* **1999**, *60*, R15021.
- (21) Di Capua, R.; Verma, M.; Radovic, M.; Strocov, V. N.; Piamonteze, C.; Guedes, E. B.; Plumb, N. C.; Chen, Y.; D'Antuono, M.; De Luca, G. M.; Di Gennaro, E.; Stornaiuolo, D.; Preziosi, D.; Jouault, B.; Miletto Granozio, F.; Sambri, A.; Pentcheva, R.; Ghiringhelli, G.; Salluzzo, M. Orbital Selective Switching of Ferromagnetism in an Oxide Quasi Two-Dimensional Electron Gas. *npj Quantum Mater.* **2022**, *71* **2022**, *7*, 41.
- (22) Piamonteze, C.; Flechsig, U.; Rusponi, S.; Dreiser, J.; Heidler, J.; Schmidt, M.; Wetter, R.; Calvi, M.; Schmidt, T.; Pruchova, H.; Krempasky, J.; Quitmann, C.; Brune, H.; Nolting, F. X-Treme Beamline at SLS: X-Ray Magnetic Circular and Linear Dichroism at High Field and Low Temperature. *urn:issn:0909-0495* **2012**, *19*, 661.
- (23) Brookes, N. B.; Yakhou-Harris, F.; Kummer, K.; Fondacaro, A.; Cezar, J. C.; Betto, D.;

- Velez-Fort, E.; Amorese, A.; Ghiringhelli, G.; Braicovich, L.; Barrett, R.; Berruyer, G.; Cianciosi, F.; Eybert, L.; Marion, P.; van der Linden, P.; Zhang, L. The Beamline ID32 at the ESRF for Soft X-Ray High Energy Resolution Resonant Inelastic X-Ray Scattering and Polarisation Dependent X-Ray Absorption Spectroscopy. *Nucl. Instruments Methods Phys. Res. Sect. A Accel. Spectrometers, Detect. Assoc. Equip.* **2018**, *903*, 175.
- (24) Kummer, K.; Fondacaro, A.; Jimenez, E.; Velez-Fort, E.; Amorese, A.; Aspbury, M.; Yakhou-Harris, F.; Van Der Linden, P.; Brookes, N. B. The High-Field Magnet Endstation for X-Ray Magnetic Dichroism Experiments at ESRF Soft X-Ray Beamline ID32. *J. Synchrotron Rad* **2016**, *23*, 464.
- (25) Stavitski, E.; de Groot, F. M. F. The CTM4XAS Program for EELS and XAS Spectral Shape Analysis of Transition Metal L Edges. *Micron* **2010**, *41*, 687.
- (26) Piamonteze, C.; Miedema, P.; De Groot, F. M. F. Accuracy of the Spin Sum Rule in XMCD for the Transition-Metal L Edges from Manganese to Copper. *Phys. Rev. B* **2009**, *80*, 184410.



TOC Graphic

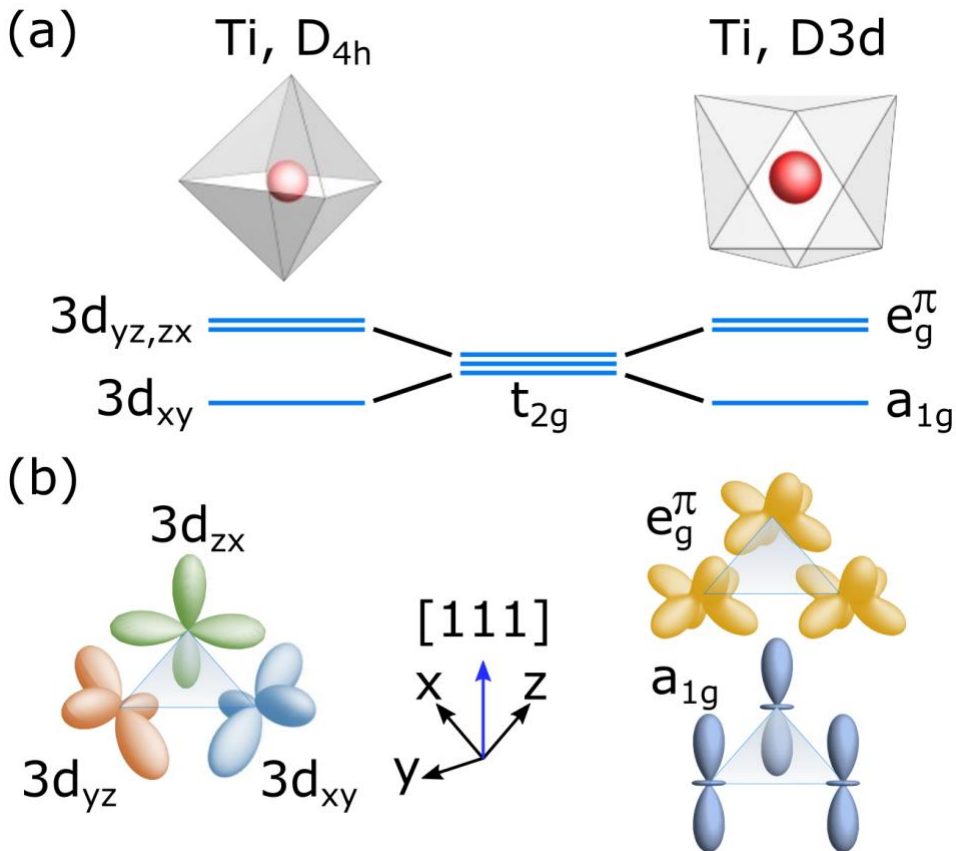


Figure 1. Schematics of crystal symmetry and orbitals. (a) A reconstruction of octahedral crystal field characterized by  $t_{2g}$  ( $3d_{xy}$ ,  $3d_{yz}$ ,  $3d_{zx}$ ) orbitals into a trigonal crystal field where  $t_{2g}$  states mix and form  $a_{1g}$  and  $e_g^\pi$  orbitals. (b) view from the (111) surface (shaded triangles) of  $D_{4h}$  and  $D_{3d}$  orbitals.

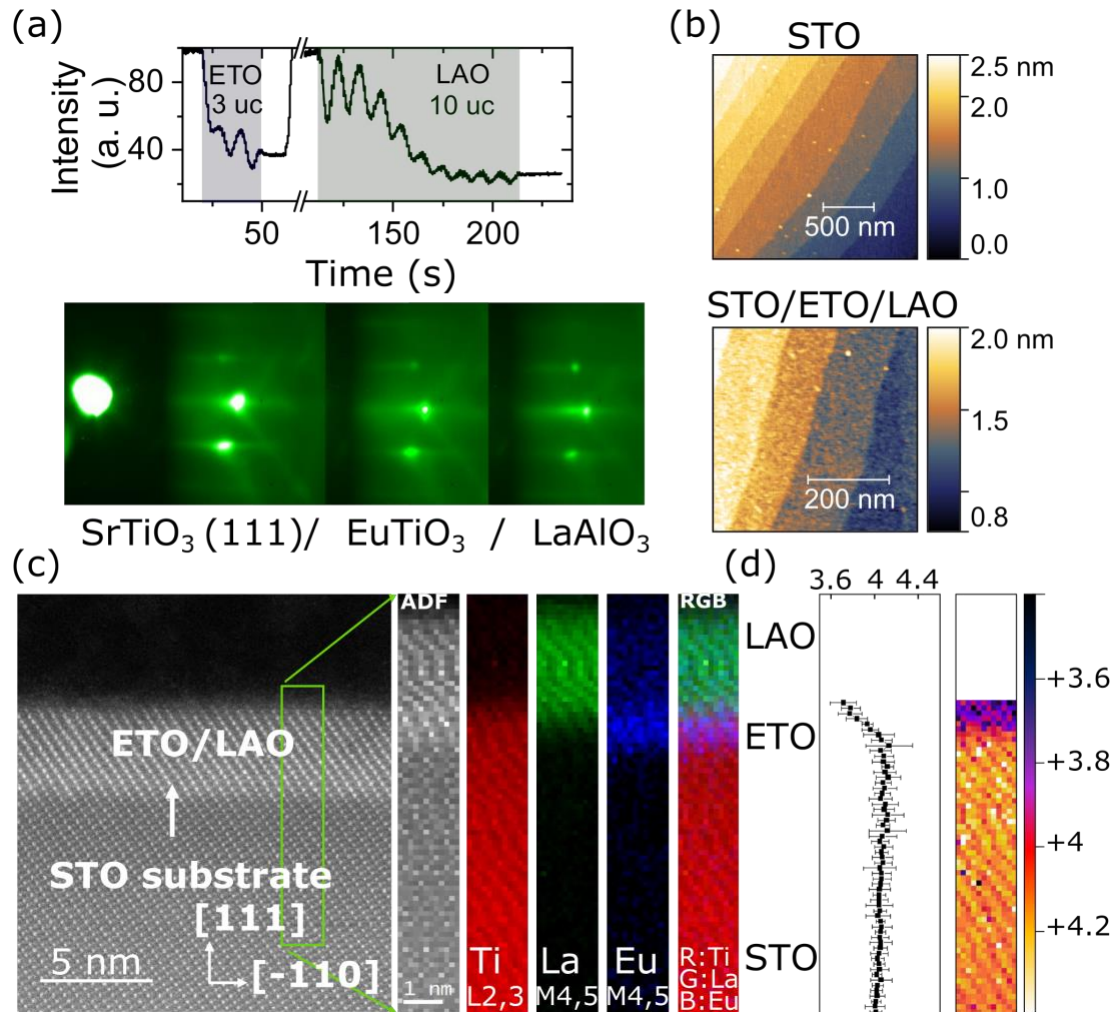


Figure 2. (a) Oscillation of RHEED intensity during the growth of a LAO/ETO/(111)STO heterostructure(upper panel) and RHEED image along the  $[10\bar{1}]$  crystallographic direction for substrate (111) STO, (111) STO/ETO and (111) STO/ETO/LAO sample. (b) AFM images of a Ti-terminated (111) STO substrate and of a (111) STO/ETO/LAO film, which show similar terrace height of 0.22-0.24 nm. (c) Annular dark field (ADF) STEM image and EELS maps of Ti, La and Eu elements. (d) A map of Ti valence by O-K near-edge EELS.

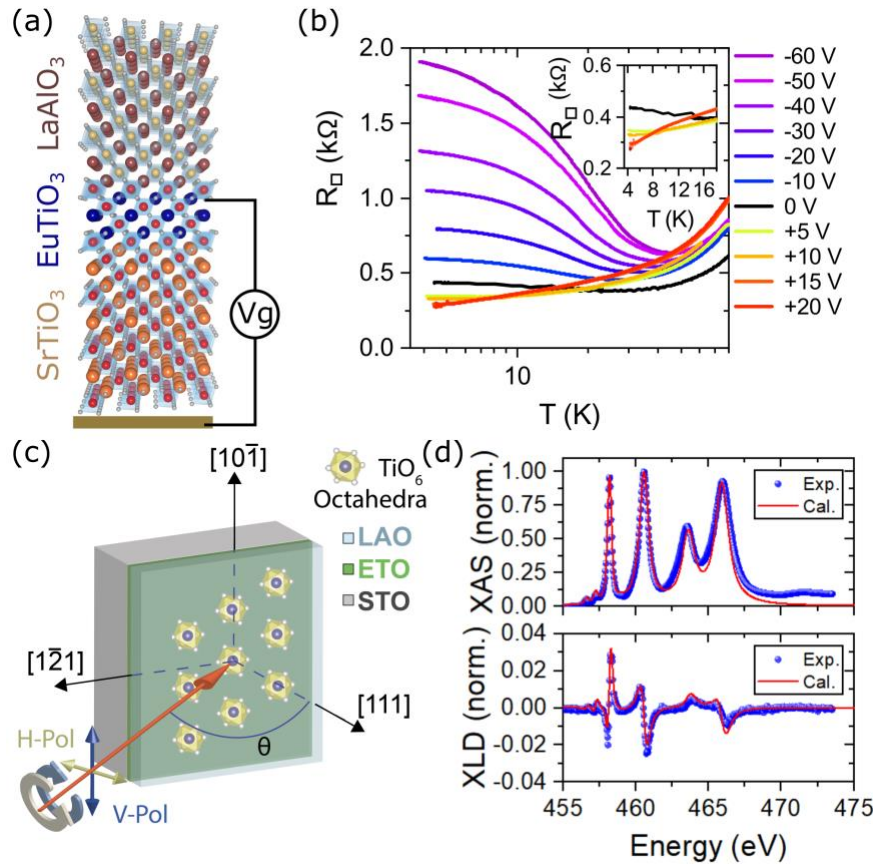


Figure 3. (a) Schematic of the (111) LAO/ETO/STO structure and of the back-gating configuration. (b) Back-gate voltage dependence of sheet resistance as a function of the temperature. In the positive voltage the downturn of resistance is zoomed in the inset. (c) Schematic of the XLD and XMCD experimental configuration. With an incidence angle  $\theta$  the x-rays (red arrow) propagate to the interface where a schematic arrangement of Ti and Oxygen ions is superimposed. The dark blue and light green arrows indicate the direction of the linear vertical and horizontal polarizations. The two circular arrows indicate right/left-handed circular polarizations. (d) Total electron yield Ti L<sub>2,3</sub> edge XAS and XLD spectra at 5K, and simulation by atomic multiplet scattering calculations using the CTM4XAS code with a D<sub>3d</sub> crystal field.<sup>25</sup> The crystal field parameters are reported in ref. [13].

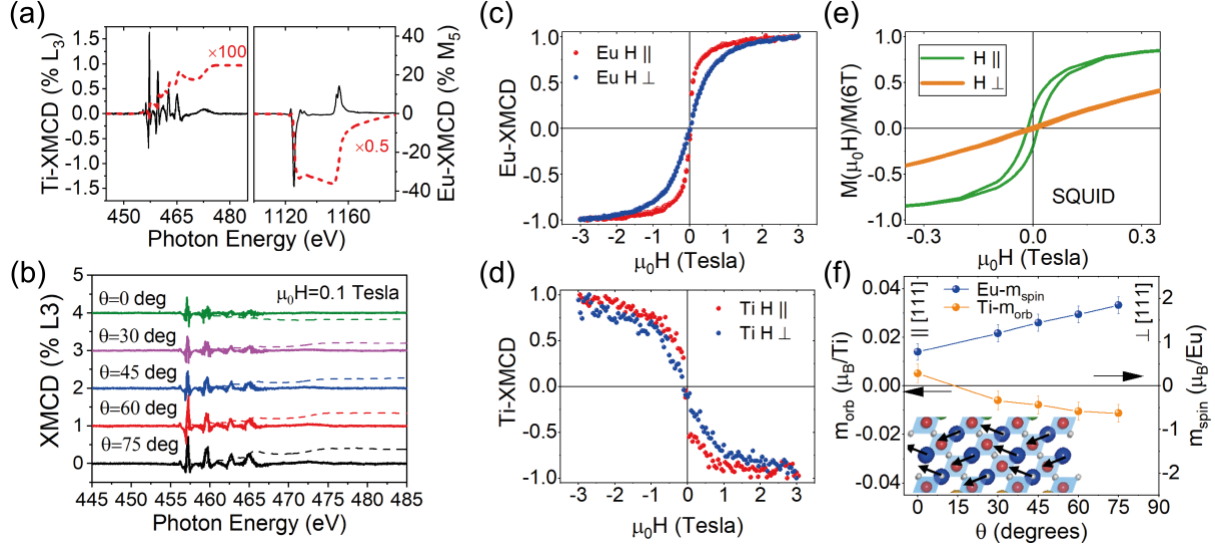


Figure 4. (a) Ti  $L_{2,3}$  edge (left panel) and Eu  $M_{4,5}$  edge (right panel) XMCD spectra acquired at 2 K and 6.5 Tesla. (b) Angular dependence of Ti-XMCD spectra (continuous lines) and their integral (dashed lines) at 0.1 Tesla. The data are displaced for clarity.  $\theta$  is the angle between the beam and surface normal. (c) Eu-XMCD  $M_5$  and (d) Ti-XMCD  $L_3$  intensities (normalized to the maximum) as function of the magnetic field parallel (red) and perpendicular (blue) to the interface. The XMCD data in parallel direction are collected in GI condition. (e) Magnetic hysteresis loop from SQUID data in parallel (green line) and perpendicular (orange line) magnetic field. (f) Eu ( $m_{spin}$ ) and Ti ( $m_{orb}$ ) magnetic moments as function of the angle  $\theta$  at 0.1 Tesla and 2 K.  $\theta=0$  degrees ( $\parallel [111]$ ) corresponds to the out-of-plane magnetic field orientation. In the inset we show a sketch of a possible non-collinear arrangement of the Eu-spin moments which leads to an in-plane ferromagnetic and an out-of-plane antiferromagnetic alignment of the spin components in the two directions (blue spheres Eu ions, red spheres Ti ions, grey spheres oxygen ions). All the magnetic measurements were performed by zero field cooling the sample down to base temperature.